

Topological obstructions in neural networks' learning

Serguei Barannikov^{a,b}, Grigorii Sotnikov^a, Ilya Trofimov^a, Alexander Korotin^a, Evgeny Burnaev^a

^a*Skolkovo Institute of Science and Technology, Moscow, Russia*

^b*IMJ, University of Paris, France*

Abstract

We apply methods of topological data analysis to loss functions to gain insights on learning of deep neural networks and their generalization properties. We study global properties of the loss function's gradient flow. We use topological data analysis of the loss function and its Morse complex to relate local behaviour along gradient trajectories with global properties of the loss surface. We define neural network's Topological Obstructions' score («TO-score») with help of robust topological invariants (barcodes of loss function) that quantify the “badness” of local minima for gradient-based optimization. We have made several experiments for computing these invariants, for small neural networks, and for fully connected, convolutional and ResNet-like neural networks on different datasets: MNIST, Fashion MNIST, CIFAR10, SVHN. Our two principal observations are 1) the neural network's barcode and TO-score decrease with the increase of the neural network's depth and width 2) there is an intriguing connection between the length of minima's segments in the barcode and the minima's generalization error.

Introduction

Mathematically, if one opens the "black box" of deep learning, there are two immediate mysteries. Firstly, the algorithms based on gradient descent achieve almost zero loss with deep neural nets although the loss functions of DNNs are non-convex, have many saddles and multiple local minima. Secondly, DNNs have good generalization properties, namely there is essentially no overfitting despite that the number of parameters in DNN is much bigger than the number of data points. To gain insights into these mysteries we propose to apply methods of topological data analysis to loss functions.

In this paper we study global properties of the loss function's gradient flow. Our main tools, which are the topological data analysis of the loss function and its Morse complex, relate local behaviour along gradient trajectories with global properties of the loss surface.

1. Barcodes of loss functions

1.1. How to quantify badness of local minima.

How to quantify to what extent a given local minimum represents an obstacle for gradient-based optimization trajectory. Clearly, some minima pose more obstacles than others (see Fig.1). Usually the badness of local minima is quantified via the Hessian. However this is often unsatisfactory. For example the two minima on Figure 1 pose different difficulty although locally they look the same.

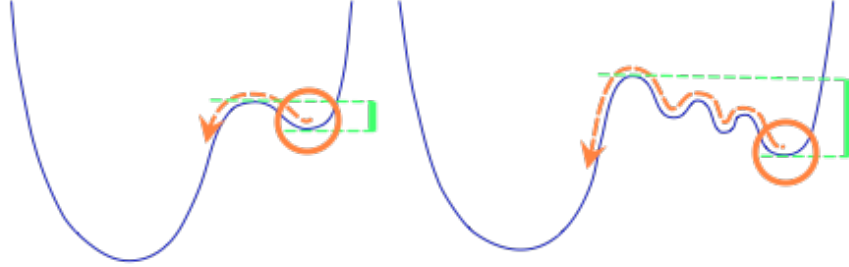


Figure 1: The two local minima, indicated by circles, look the same locally, but pose quite different difficulty to gradient-based optimization. The difficulty is quantified by the lengths of the green segments, which are attached to these minima in Barcode (L)

Barcodes are precisely the numerical invariants that quantifies badness of each local minimum.

To escape a vicinity of a given local minimum p , a path starting at p has to climb up on loss landscape. However climbing up to closest ridge point from which the path can then go down in direction of another minimum, does not guarantee that such path descends to a point with loss lower than $L(p)$. For any local minimum p there is the minimal height ($L(p)$ plus "penalty") to which a path starting at p has to climb, before it can reach a point with loss *lower* than $L(p)$ (see Fig.1).

Definition. Consider various paths $\gamma : [0, 1] \rightarrow \Theta$ starting from local minimum p and going to a point with loss **lower** than $L(p)$. Let $m_\gamma \in \Theta$ be the maximum of the loss L on such path γ . Let h_p be the minimal value of m_γ , or the height corresponding to the smallest "penalty" for going to lower loss points starting from p :

$$h_p = \min_{\gamma: [0, 1] \rightarrow \Theta, \gamma(0)=p, L(\gamma(1)) < L(p)} \max_t L(\gamma(t)) \quad (1)$$

We associate with local minimum p the segment $s_p = [L(p), h_p]$. The segment's length represents the minimal obligatory penalty for reaching lower loss points starting from p .

Definition. ([1]) The barcode of minima for loss function is the disjoint union of the segments s_p for local minima p , plus half-line accounting for the global minimum

$$\text{Barcode} (L) = [L(p_{\text{global}}), +\infty) \sqcup (\sqcup_p [L(p), h_p]) \quad (2)$$

The bigger the length of this segment the more difficult for gradient-based optimization trajectory trapped in vicinity of p to escape it and to reach lower loss values.

Saddles of small indexes and flat regions in vicinity's of them can also pose obstacles for gradient-based optimization. All these obstacles are topological in nature, as any critical point or critical manifold. We describe in Appendix H the analogous topological invariants, barcodes of higher indices, quantifying "lifetimes" of saddles (see [1]).

1.2. Barcodes via gradient flow on segments. Algorithm

In terms of gradient flow the barcode of minima can be calculated via the formula (1) as follows.

Let $s(t)$, $t \in [0, 1]$ be a path from a local minimum p to a lower value minimum p' . Consider action of the gradient flow

$$\dot{\theta} = -\text{grad } L$$

on the path s , up to reparametrization of the curve. At each path's point t the gradient $\text{grad } L$ is decomposed into sum

$$-\text{grad } L = (-\text{grad } L)_{\parallel} + (-\text{grad } L)_n$$

of two components, where $(-\text{grad } L)_{\parallel}$ is parallel to the tangent vector to $s(t)$ and $(-\text{grad } L)_n$ is orthogonal to it. The action by tangent component $(-\text{grad } L)_{\parallel}$ is absorbed into reparametrization of path $s(t)$. The gradient flow moves the curve $s(t)$ by $(-\text{grad } L)_n$, the normal component of $-\text{grad } L$.

In realization we optimize the curve by applying the orthogonal gradient $(-\text{grad } L)_n$, multiplied by learning rate, to a set of points approximating $s(t)$. The maximum value of the loss function on the set of points approximating $s(t)$ decreases, for sufficiently small learning rate, at each iteration. For Lipschitz L and sufficient number of points this also ensures that

$$L_{\max}(s) = \max_t L(s(t))$$

the maximal value on the curve decreases. Details of this optimization on sampled paths are described in section 2 below. In the cases of extremely high dimensional deep neural networks if the computation of $(-\text{grad } L)_n$ on sufficiently big number of points approximating a curve becomes prohibitively expensive, the following strategy can be applied: replace the computation of $(-\text{grad } L)_n$ for a big number of points on the curve by stochastic estimate via calculation on fewer number of points distributed randomly along the curve.

After optimizing a set of sampled paths starting at given minimum p and going to points with lower loss, we calculate the segment corresponding to p in Barcode (L) using formula (1). This is summarized in Algorithm 1 below.

Algorithm 1: Barcode of minima computation for loss function of DNN.

```

 $S_0 \leftarrow \{\text{Optimized sampled points (minima)} p \in \Theta\}$ 
Barcode  $\leftarrow \emptyset$ 
for  $p \in S_0$  in increasing order of  $L(p)$  do
   $b[p] \leftarrow L(p)$ 
   $h[p] \leftarrow +\infty$ 
  for  $(q \in S_0) \ \& \ (L(q) < L(p))$  do
     $\gamma(t) \leftarrow \text{Optimized sampled path } \gamma, \gamma(0) = p, \gamma(1) = q$ 
     $h[p] \leftarrow \min(h[p], \max_{t \in [0,1]} L(\gamma(t)))$ 
  end
  Barcode  $\leftarrow \text{Barcode} \sqcup [b[p], h[p]]$ 
end
return Barcode

```

This algorithm gives a stochastic estimate for Barcode (L) .

1.3. Topological obstructions (TO-) score

In the ideal situation, if loss function has single minimum and no other local minima and $(\text{grad } L)|_{\partial\Theta}$ is pointing outside of Θ , then all gradient trajectories $\dot{x} = -\text{grad } L$ for all starting points, except for a set of measure zero, always converge to the single minimum.

We define neural network's **Topological obstructions (TO-) score** as the distance between the minima's barcode of the neural network's loss function L and the minima's barcode of such ideal function L^{ideal} with the single minimum at the same level as the value of the global minimum of L :

$$\text{TO Score} = \text{Distance}(\text{Barcode}(L), \text{Barcode}(L^{\text{ideal}})) \quad (3)$$

The distance here is the standard **Bottleneck distance** [2] (also known as Wasserstein- ∞ distance \mathbb{W}_∞) on the corresponding persistence diagrams (2-dimensional point clouds of birth-death pairs, with points $(l, +\infty)$ represented as separate 1-dimensional point cloud):

$$\mathbb{W}_\infty(\mathcal{D}, \mathcal{D}') := \inf_{\pi \in \Gamma(\mathcal{D}, \mathcal{D}')} \sup_{a \in \mathcal{D} \cup \Delta} |a - \pi(a)|. \quad (4)$$

Here Δ denotes the "diagonal" (pairs with birth equal to death) and $\Gamma(\mathcal{D}, \mathcal{D}')$ denotes the set of partial matchings between \mathcal{D} and \mathcal{D}' defined as bijections between $\mathcal{D} \cup \Delta$ and $\mathcal{D}' \cup \Delta$.

1.4. Lifetimes of saddles. Calculation of r -saddles barcode via gradient descent on simplexes

Here we describe analogous calculation of barcodes for saddles of arbitrary index $r \geq 1$. These barcodes quantify the index r saddles' "lifetimes".

For this calculation one first optimizes sampled r -simplices. This is similar to optimization of sampled 1-simplices as described in section 1.1. At each interior point of the simplex the gradient $\text{grad } L$ is decomposed into sum

$$-\text{grad } L = (-\text{grad } L)_{\parallel} + (-\text{grad } L)_n$$

of two components, where $(-\text{grad } L)_{\parallel}$ is parallel to the simplex's tangent plane and $(-\text{grad } L)_n$ is orthogonal to it. The action by tangent component $(-\text{grad } L)_{\parallel}$ is absorbed into reparametrization of the simplex. The gradient flow moves the simplex by $(-\text{grad } L)_n$, the normal component of $-\text{grad } L$.

The set of optimized r -simplices is constructed inductively starting from a set of optimized sampled 0-simplices (minima), then the optimized 1-simplices for each pair of minima; then the optimized 2-simplex for every triple of sampled minima etc.

After optimizing a set of sampled r -simplices, a filtration is constructed on this set of simplices using the maximal value of loss on the given simplex. The linear boundary operator ∂_r acts on the linear space formally generated by simplices by sending a simplex to the alternated sum of its $(r-1)$ -faces. Next the filtration is used to bring the boundary linear operator ∂_r to its canonical form. This gives the birth and death values for segments in the index- r barcode ([1]).

The index r TO-score for index r barcodes is defined by the same formula (3), where L^{ideal} is an ideal function without critical points except for the global minimum. Zero TO-scores for all indexes indicates that the loss function, after a change of parametrization in Θ , can be made convex.

1.5. Lowering of barcodes with increase of depth and width of network

The neural networks which we consider can be embedded into similar networks, which are wider and/or deeper, and which have more parameters. An increase of number of parameters leads to lowering of value of given minimum, which gets a possibility to descent lower in new directions.

It turns out that in the considered networks the barcodes of minima also get lower.

We demonstrate the phenomena of barcodes' lowering with increase of network depth and width on the MNIST, FMNIST datasets with fully-connected neural networks with 2,3,4,6 and 8 hidden layers in section 2.1, and on CIFAR10 dataset in section 2.2 with convolutional neural networks CNN32-1,CNN32-2,CNN32-3,CNN64-1,CNN64-2,CNN128-1.

2. Experimental part

2.1. Experiments demonstrating the lowering of barcodes with increase of neural network depth

We show in this section how the barcodes are calculated by the proposed procedure (Algorithm 2) and demonstrate the lowering of barcodes with increase of the neural networks depth. Moreover the height of segment from barcode is a topological characteristics of the minimum which is correlated with the generalization error of given minimum compared to minima obtained using other optimization parameters.

Fully connected neural networks. We demonstrate the lowering of barcodes on MNIST and FMNIST datasets using fully connected neural networks with 2,3,4,6 and 8 layers with 32 neurons in each layer. Randomly chosen 10 minima were trained until full convergence, using Adam [4] and Cyclical Learning Rate [6]. Each pair of minima was connected by a curve in the form of line segment. Then the training procedure described above in section was applied to the curve. After the low loss connecting curve is obtained, for each curve the maximal value of loss is found and then for each of minima the lowest value maximum on such curves is calculated. Then the segment gives the segment corresponding to the given minimum in the barcode.

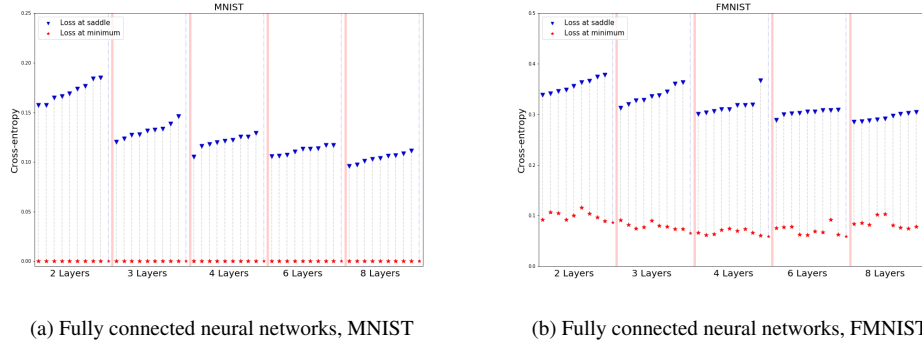


Figure 2: Barcodes of deep neural network (consisting of 2, 3, 4, 6, 8 layers) loss surfaces.

2.2. Convolutional neural networks

To evaluate the hypothesis we have experimented with various CNN architectures on the well-known CIFAR10 dataset. For this purpose we have used fairly simple networks, containing one, two and three convolutional layers, both with and without Batch Normalization before activation function. To emphasize on the connection between height of the saddle and convolutional layers we have made the number of parameters in fully-connected layer dependent only on the number of channels in convolutional layers (remains fixed among all of them). To make it possible, max-pooling operation is extensively used, details can be found in Table E.8.

Algorithm 2: Optimize path

```
Procedure proj( $\theta_i, \theta_j$ ):
    return  $\frac{\theta_i - \theta_j}{\|p_i - p_j\|}$ 
Procedure STEP(path,  $x$ ):
     $i \leftarrow 1$ 
    while  $i < |\text{path}| - 1$  do
         $\theta_l \leftarrow \text{path}_{i-1}$ 
         $\theta_c \leftarrow \text{path}_i$ 
         $\theta_r \leftarrow \text{path}_{i+1}$ 
         $\nabla f_{\theta_c} = \nabla_{\theta_c}(\mathcal{L}(f_{\theta_c}, x))$ 
         $\nabla^{left} f_{\theta_c} = \langle \nabla f_{\theta_c}, \text{proj}(\theta_c, \theta_l) \rangle \cdot \text{proj}(\theta_c, \theta_l)$ 
         $\nabla^{right} f_{\theta_c} = \langle \nabla f_{\theta_c}, \text{proj}(\theta_r, \theta_c) \rangle \cdot \text{proj}(\theta_r, \theta_c)$ 
         $\text{path}_i \leftarrow \theta_c - \eta(\nabla f_{\theta_c} - \frac{\nabla^{left} f_{\theta_c} + \nabla^{right} f_{\theta_c}}{2})$ 
         $i \leftarrow i + 1$ 
    end
return path
```

2.3. Decrease of saddle height with complexity increase

As it was mentioned in prior works BN has a smoothing effect on the loss function. Figure 3 helps to evaluate this statement. We see that among CNNs of all considered depth, their counterparts with BN have both lower loss values in local minimas and in saddle points, which is especially clear in case of CNN-3. It can be understood from the position that initial points of the path, being initialized on a segment may have completely irrelevant parameters in early convolutional layers, inducing instability in activations which is later corrected by Batch Normalization.

Our experiments presented in the Figure 4 show that connection between the architecture of a network and value of corresponding loss function in saddle point is established in a very intuitive way. Namely, it can be decreased both by increasing the number of convolutional layers or number of channels in them. On the left part we see monotonic decrease of loss function's value in found saddle point due to increase of channels number in a single convolutional layer. Moreover, on the right part it is distinguishable that even more rapid drop after adding new convolutional layers. Here we sort architectures w.r.t. number of parameters in them and see a straightforward dependence. However this is not always true and this effect is local as increasing the number of parameters in a simple architecture will lead to plateau of loss function's values, i.e. saturation of considered effect.

2.4. Connection between barcodes and generalization.

To investigate the connection between height of the saddle and generalization properties of obtained minimums we have considered the work [5].

There the designed experiment on CIFAR10 showed that neural networks trained with constant small learning rate have less test accuracy compared to ones, trained with a higher learning rate, being annealed during the training process. The authors provide evidence that it is the effect of presence of easy-to-generalize, hard-to-fit patterns in the dataset, which are commonly learned with small learning rate, on the other hand, when starting with a larger one, they are being initially ignored and at first and easy-to-fit, hard-to-generalize patterns attract sufficient amount of attention.

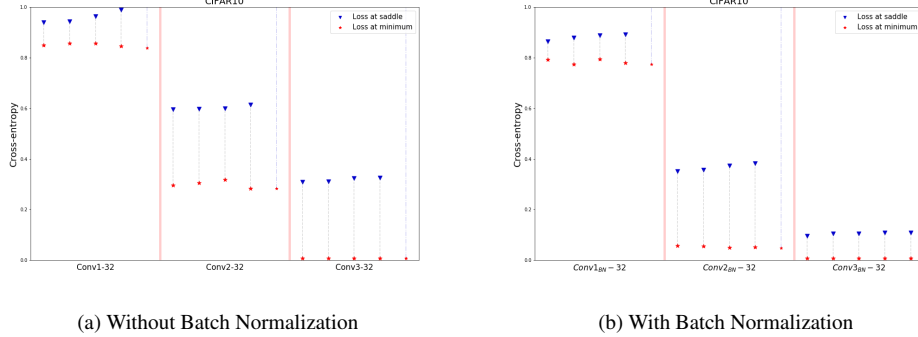


Figure 3: Effect of Batch Normalization on the height of saddles.

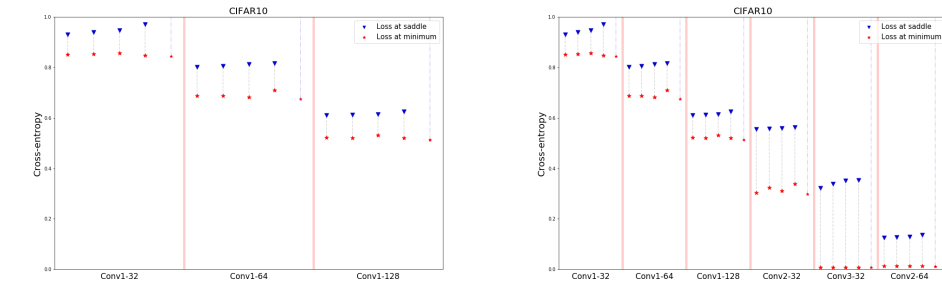


Figure 4: Effect of increase of parameters number on barcodes.

To explore this phenomenon from a different perspective we have analyzed the loss function for both types of these minimums.

2.5. Training

First and foremost, 8 ResNet-like [3] models were trained on CIFAR10 in two scenarios to obtain a closer match with the results of the authors: using a constant small learning rate (10^{-4}) and applying annealing of learning rate (starting from 10^{-2} and ending with 10^{-4}). The goal of the training process was to achieve the lowest possible loss on the training set. That's why at that point we have obtained two groups of minimums with similar, nearly zero values of loss function on the training set, however their test accuracy differed significantly: 67.4% vs 75.7% giving a sense about huge generalization gap of the first types of minimums compared to the second. It's important to mention, that to grasp the considered effect, we have trained models without using any form of regularization. Further training details can be found in appendix.

2.6. Optimization

Initially minimums were connected by straight segments on which we have selected points with equal distance between each other. Our experiments showed that for different types of model's architectures and datasets their number may vary. The most undesired behavior of path during optimization process will be faced when the number of points doesn't match the complexity of the model, especially when it is too small. It will lead to the situation when directly optimized points converge to the local optima and achieve low regions of loss function by the cost of becoming distant from each other. Due to the complexity of loss surface the structure of the path will be lost in that case.

In order to evaluate the values of loss function between optimized points of the path, the linear interpolation between them was used.

Then a continuous set of values representing loss along path may be written as $\cup_{i=1}^{|path|} L(f, (1 - \alpha)\theta_i + \alpha\theta_{i+1}, D)$, where $\alpha \in [0, 1]$.

Algorithm 3: Refine path

Procedure $\text{INSERTION}(path, criterion)$:

```

 $\mu \leftarrow \frac{\|\theta_{last} - \theta_{first}\|_2}{|path|}$ 
 $L_{max} \leftarrow \max_i(L(\theta_i)_{f,D})$  where  $i \in [0, |path| - 1]$ 
 $T \leftarrow 1.2$ ,  $i \leftarrow 0$ ,  $B \leftarrow \text{array}()$ ,  $D \leftarrow \text{array}()$ 
while  $i < |path| - 1$  do
     $D[i] \leftarrow criterion(\theta_i, \theta_{i+1})$ 
     $i := i + 1$ 
end
if  $\max(D) > T$  then
     $max_1 \leftarrow \text{argmax}_i(D)$ 
     $max_2 \leftarrow \text{argmax}_j(D \setminus \max(D))$ 
     $path[max_1] \leftarrow \frac{\theta_{max_1} + \theta_{max_1+1}}{2}$ 
     $path[max_2] \leftarrow \frac{\theta_{max_2} + \theta_{max_2+1}}{2}$   $\triangleright$  Length  $|path| \uparrow 2$ 
     $B \leftarrow path_0, path = path \setminus path_0$ 
     $B \leftarrow path_{|path|}, path = path \setminus path_{|path|}$   $\triangleright$  Length  $|path| \downarrow 2$ 
end
return path, B
Procedure  $loss\ criterion_{L_{max}}(\theta_i, \theta_{i+1})$ :
 $loss = L((1 - \alpha)\theta_i + \alpha\theta_{i+1})_{f,D}$ , where  $\alpha \in (0, 1)$ 
return  $\frac{\max(loss)}{L_{min}}$ 
Procedure  $distance\ criterion_{\mu}(\theta_i, \theta_{i+1})$ :
return  $\frac{\|\theta_i - \theta_{i+1}\|_2}{\mu}$ 

```

In our set up we have came up with a number of 19 points, connecting a pair of minimums. Experimentally we show that picking larger number does not give an improvement without a carefully tuned point insertion/rejection procedure which is shown in the Figure F.7. Also we discovered that L_2 regularization on parameters θ_j (single point belonging to the optimized path) has positive effect on optimization process as generally prevents points from moving far from the origin and as a result constrains pairwise distance. Every 25 epochs the decision was made via

Algorithm 3 whether to insert new points preserving the structure of the path in it's particular region or it is not necessary.

Insertion procedure is applied in combination with one of two proposed criterions, based on loss or distance between optimized points. In case of loss criterion, the situation is clear as revealing high values between optimized points our natural reaction is to insert additional point in that region to bypass the peak. However by doing that we may harm the structure of the path by producing superior density of points in a particular region of loss function. Our observations showed that frequently high loss between optimized points is a result of them becoming more distant from each other than they are considered to be, then we can set an upper bound on distance between them and by adding intermediate points maintain the structure of the path.

2.7. Connection between saddle height and generalization

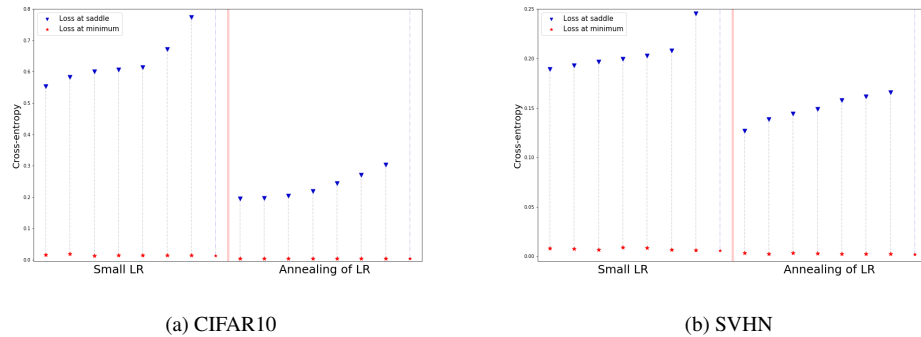


Figure 5: Difference of loss function's values in saddle points of local minimums trained with a constant small learning rate (left from the red line), with annealing of learning rate (right from the red line).

As a result, this experiment implied optimizing 28 paths between pairs of minimums of type 1 and also type 2. Considering the procedure stated in Chapter 1, Barcodes were calculated based not only on the optimized points but also on intermediate points, lying on the straight segments connecting optimized points. To perform such evaluation, following set of values $\alpha \in [0.2, 0.4, 0.6, 0.8]$ was considered. We observe that loss at the saddle points for minimums of the first time are always higher than for it's counterpart. To approve this result we have also completed the same procedure for SVHN dataset and faced conceptually the same outcome.

It tells us that even if models have nearly the same training loss, their generalization potential can be quantified by calculating barcodes and thus make a decision to use a model with a lower one as it indicates higher generalization guarantees. Though this process is very computationally costly and for now can not be effectively scaled across too complex architectures and large-scale-datasets.

3. Conclusion

In this work we have outlined several important observations about Deep Neural Network's loss function, which were stated theoretically and later evidence was provided experimentally. What is more, we have obtained a practical strategy to apply proposed methods on arbitrary dataset with a wide range of architectures for any differentiable loss function and established a

pipeline on an image classification task. A practical use of our results is straightforward as it can be applied in the meaning of a tool to compare trained models w.r.t. their topological properties as they proved to be highly correlated with the generalization potential of a given model. As an outcome, barcodes, calculated via proposed procedure may be helpful in several tasks as they enlarge our knowledge about the model.

Appendix A. Finding local minima

During networks training we used the following learning rate scheduler:

$$S(m_1, m_2, lr^{max}, lr^{min}, i) = \begin{cases} lr^{max}, & \text{if } batch_i \leq |D|m_1 \\ (1 - \Delta_i) \cdot lr^{max} + \Delta_i \cdot lr^{min}, & \text{if } |D|m_1 < batch_i < |D|m_2 \\ lr^{min}, & \text{if } batch_i \geq |D|m_2 \end{cases}$$

Where $|D|$ - number of batches in the dataset and $\Delta_i = \frac{batch_i - |D|m_1}{|D|(m_2 - m_1)}$.

Note that in such formulation $S(0, 0, 0, lr_0, lr_0)$ will correspond to the simplest case, when the learning rate is fixed to the value lr_0 during the whole training process and let's denote it $S(lr_0)$ for simplicity. It implies changing learning rate after every batch if necessary.

Table A.1: CIFAR10 Training parameters

Type	Optimizer	BS	$\ \theta\ _2$	Scheduler	Epochs	
1	SGD, $\nu=0.9$	256	0	$S(10^{-4})$	1500	
2	SGD, $\nu=0.9$	256	0	$S(10, 80, 10^{-2}, 10^{-4}, \cdot)$	300	

Table A.2: SVHN Training parameters

Type	Optimizer	BS	$\ \theta\ _2$	Scheduler	Epochs	
1	SGD, $\nu=0.9$	256	0	$S(10^{-4})$	1500	
2	SGD, $\nu=0.9$	256	0	$S(50, 100, 5 \cdot 10^{-2}, 10^{-4}, \cdot)$	100	

Appendix B. Visual interpretation of insertion procedure

We motivate proposed insertion procedure with the following example on the model data. At the first stage two points were optimized and they ended in reasonable regions of loss function with low loss values. However it is visually noticeable that linear interpolation between them will produce points completely off the desired manifold, preserving low values of loss function. But applying our procedure, by adding new points and optimizing them, they will reach relevant region and we can get rid of such negative effect.

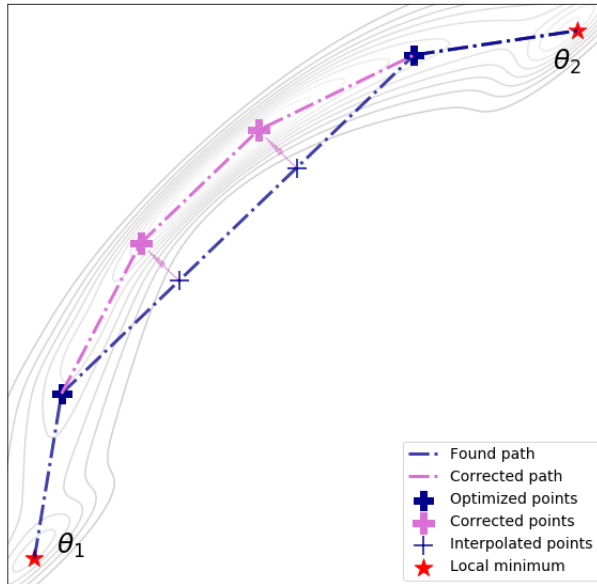


Figure B.6: Illustration of point insertion

Appendix C. Characteristics of local minimums

Table C.3: CIFAR10 minimums characteristics

Type	Train loss	Test loss	Train accuracy, %	Test accuracy, %
1	0.01 ± 10^{-3}	1.74 ± 0.058	100 ± 0	67.41 ± 0.93
2	0.001 ± 10^{-4}	1.32 ± 0.033	100 ± 0	75.74 ± 0.64

Table C.4: SVHN minimums characteristics

Type	Train loss	Test loss	Train accuracy, %	Test accuracy, %
1	0.01 ± 10^{-3}	0.53 ± 0.025	100 ± 0	88.12 ± 0.40
2	0.001 ± 10^{-4}	0.42 ± 0.015	100 ± 0	93.29 ± 0.19

Appendix D. Optimization of Path

While calculating Barcodes for CIFAR10 the following hyperparameters were used in combination with Distance Criterion, responsible for efficiently preserving the structure of a path.

Table D.5: CIFAR10 Path optimization hyperparameters

Optimizer	Batch size	$\ \theta\ _2$	Scheduler	Epochs
SGD, $\nu=0$	150	10^{-5}	$S(270, 300, 2 \cdot 10^{-3}, 1.25 \cdot 10^{-4}, \cdot)$	300

Table D.6: SVHN Path optimization hyperparameters

Optimizer	Batch size	$\ \theta\ _2$	Scheduler	Epochs
SGD, $\nu=0$	256	10^{-5}	$S(170, 200, 2 \cdot 10^{-3}, 1.25 \cdot 10^{-4}, \cdot)$	200

Appendix E. Architectures of used networks.

In case of the second experiment a simplified lightweight ResNet-like architecture, containing 195k trainable parameters was used.

Table E.7: Architecture of ResNet used in the 2 experiment.

ResNet
$x^0 = \text{Conv}(3, 16, 3 \times 3), \text{ReLU}$
$x^1 = \text{Conv}(16, 16, 3 \times 3), \text{ReLU}, \text{Conv}(16, 16, 3 \times 3) + x^0$
$x^2 = \text{MaxPooling}(2 \times 2), \text{Conv}(16, 32, 3 \times 3), \text{ReLU}$
$x^3 = \text{Conv}(32, 32, 3 \times 3), \text{ReLU}, \text{Conv}(32, 32, 3 \times 3) + x^2$
$x^4 = \text{MaxPooling}(2 \times 2), \text{Conv}(32, 64, 3 \times 3), \text{ReLU}$
$x^5 = \text{Conv}(64, 64, 3 \times 3), \text{ReLU}, \text{Conv}(64, 64, 3 \times 3) + x^4$
$x^6 = \text{MaxPooling}(2 \times 2), \text{Conv}(64, 64, 3 \times 3), \text{ReLU}$
$x^7 = \text{Conv}(64, 64, 3 \times 3), \text{ReLU}, \text{Conv}(64, 64, 3 \times 3) + x^6$
$x^8 = \text{MaxPooling}(2 \times 2), \text{BatchNorm}(64)$
$\hat{y} = \text{Linear}(X^8, 10)$

Table E.8: Architecture of CNN-1-C used in the 1 experiment.

CNN-1-C
$x^0 = \text{Conv}(3, C, 5 \times 5), \text{ReLU}$
$x^1 = \text{MaxPooling}(8 \times 8)$
$\hat{y} = \text{Linear}(16 \cdot C, 10)$

Table E.9: Architecture of CNN-2-C used in the 1 experiment.

CNN-2-C
$x^0 = \text{Conv}(3, C, 5 \times 5), \text{ReLU}$
$x^1 = \text{MaxPooling}(2 \times 2)$
$x^2 = \text{Conv}(C, C, 5 \times 5), \text{ReLU}$
$x^3 = \text{MaxPooling}(4 \times 4)$
$\hat{y} = \text{Linear}(16 \cdot C, 10)$

Table E.10: Architecture of CNN-3-C used in the 1 experiment.

CNN-3-C
$x^0 = \text{Conv}(3, C, 5 \times 5), \text{ReLU}$
$x^1 = \text{MaxPooling}(2 \times 2)$
$x^2 = \text{Conv}(C, C, 5 \times 5), \text{ReLU}$
$x^3 = \text{MaxPooling}(2 \times 2)$
$x^4 = \text{Conv}(C, C, 5 \times 5), \text{ReLU}$
$x^5 = \text{MaxPooling}(2 \times 2)$
$\hat{y} = \text{Linear}(16 \cdot C, 10)$

Appendix F. Example illustrating sub-optimallity of path search without point insertion

This experiment represents the situation, when we start to optimize 100 intermediate points of the path from beginning. It is noticeable that even when the number of point is large, the behaviour of loss function between the optimized points is very unstable.

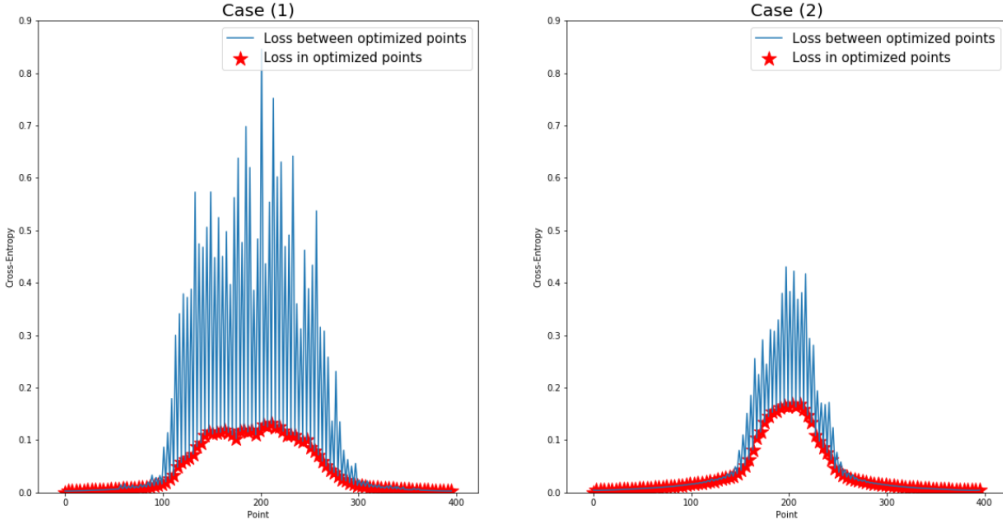


Figure F.7: CIFAR10, exp2

Appendix G. Characteristics of optimized path

Norm of gradient's tangent projection in every point of a single path, averaged across an epoch at different moments of training. During training we see a rapid drop in the middle, that indicates the flatness of this region of loss function.

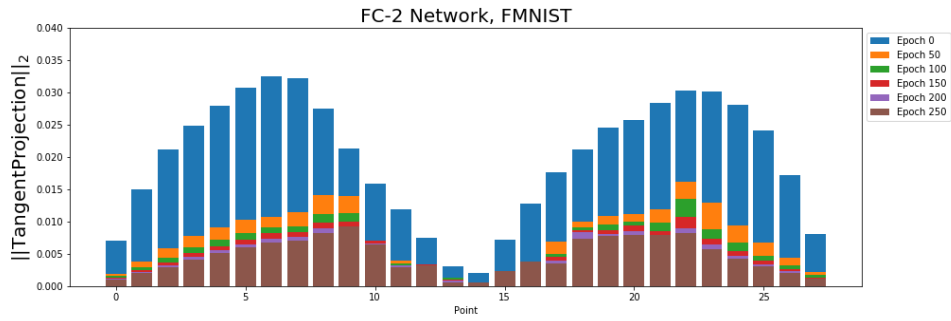


Figure G.8: Norm of tangent projection during optimization

To illustrate the process of convergence of a single path, in each point, the norm of orthogonal gradient is accumulated after several epochs. We see that at the end of training the values are much lower and nearly zero, telling us that the points of obtained path nearly found flat regions of loss surface and will not change much after optimization.

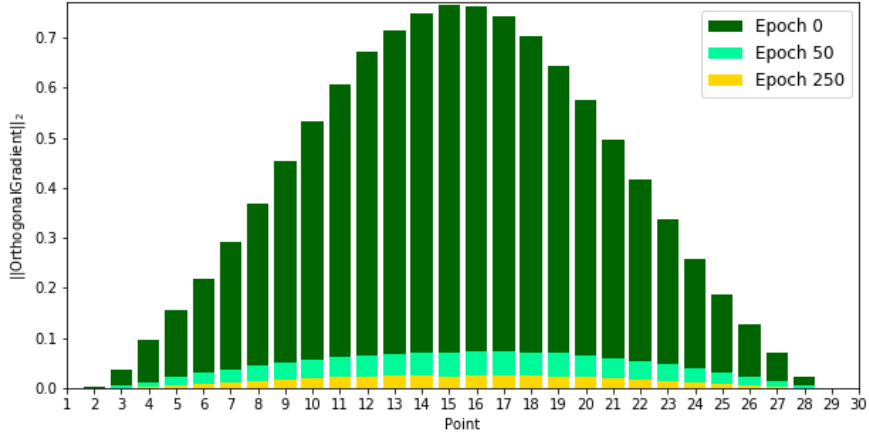


Figure G.9: Norm of orthogonal gradient

Appendix H. Introduction to Morse complex and its invariants

Morse theory principal notions are critical points and gradient flow trajectories. Optimization algorithms' two main notions are essentially parallel: minima and gradient descent trajectories.

Here for the sake of geometric intuitivity we describe our topological invariants under assumption that the loss is a generic smooth function. Modifications for continous piece-wise smooth loss are immediate and are briefly described at the end of this section.

Definition. A point p is a critical point if the gradient at p is zero: $df|_p = 0$. A critical point p is non-degenerate if the Hessian matrix of f at p is non-degenerate. The index of a non-degenerate critical point is the dimension of the Hessian's negative subspace.

A gradient flow trajectory $x(t)$, $t \in [t_0, +\infty)$ is a solution to

$$\dot{x} = -\nabla f(x) \quad (\text{H.1})$$

A nondegenerate critical point of index k is also called k -saddle. Near such point the function can be written in some coordinates as

$$f = -x_1^2 - \dots - x_k^2 + x_{k+1}^2 + \dots + x_n^2. \quad (\text{H.2})$$

Saddles of small index play important role in the gradient descent optimization algorithms. The gradient descent trajectories are attracted by such points, and more generally by critical manifolds of small index. Gradient trajectories spend long periods of time in a vicinity of such points while trying to find one of the few descending, i.e. negative for the Hessian, directions.

The gradient flow trajectories can be extended back either to converge in the limit $t \rightarrow -\infty$ to a critical point, or to start from a point at the boundary of parameter domain. Here we assume for simplicity that the gradient of f at each point of the boundary of the domain Θ is pointing inside the domain. For each point with nonzero gradient there is a unique gradient flow trajectory passing through this point. This gives a decomposition of the parameter domain.

The set of all points which lie on gradient flow trajectories converging to this critical point in the limit $t \rightarrow -\infty$, is diffeomorphic to a ball of dimension k , where k is the index of the critical point. Indeed, first notice that locally near the given critical point of index k the set of such points lying on gradient flow trajectories emanating from this critical point is diffeomorphic to a ball of dimension k . Next this diffeomorphism can be extended to the set of all points lying on gradient flow trajectories emanating from this critical point, using the gradient flow. Similarly the union of all trajectories emanating from boundary of the parameter space is diffeomorphic to $S^{N-1} \times \mathbb{R}$.

Therefore the parameter space decomposes into cells of uniform flow. Each cell is formed by all gradient flow trajectories converging in the limit $t \rightarrow -\infty$ to a given critical point.

Morse complex records how these cells are glued to each other to form the total parameter space.

Let

$$\mathcal{M}(p_\alpha, p_\beta) = \left\{ \gamma : \mathbb{R} \rightarrow M^n \mid \dot{\gamma} = -(\text{grad}f)(\gamma(t)), \lim_{t \rightarrow -\infty} \gamma = p_\alpha, \lim_{t \rightarrow +\infty} \gamma = p_\beta \right\} / \mathbb{R}$$

be the set of gradient trajectories connecting critical points p_α and p_β ,

If $\text{index}(p_\beta) = \text{index}(p_\alpha) - 1$ then generically the set $\mathcal{M}(p_\alpha, p_\beta)$ is finite. Let $\#\mathcal{M}([p_\alpha, \text{or}], [p_\beta, \text{or}])$ denotes in this case the number of the trajectories, counted with signs taking into account a choice of orientation, between critical points p_α and p_β . Here we have fixed a choice of orientation "or" of negative hessian subspace at each critical point.

Let ∂_j denotes the matrix with entries $\#\mathcal{M}([p_\alpha, \text{or}], [p_\beta, \text{or}])$. In other words ∂_j is the linear operator defined by

$$\partial_j [p_\alpha, \text{or}] = \sum_{\text{index}(p_\beta)=j-1} [p_\beta, \text{or}] \#\mathcal{M}(p_\alpha, p_\beta)$$

An important property of matrices ∂_j is that their consecutive composition is zero

$$\partial_j \circ \partial_{j-1} = 0$$

This can be proven by looking at families of gradient flow trajectories connecting critical points with indexes $\text{index}(p_\beta) = \text{index}(p_\alpha) - 2$. Generically such family is one-dimensional and compact, and therefore it is a disjoint union of circles and segments. The result follows then from each segment having two boundary points so that the corresponding composite trajectories naturally cancel each other.

References

- [1] S. Barannikov. Framed Morse complexes and its invariants. *Adv. Soviet Math.*, 22:93–115, 1994.
- [2] Alon Efrat, Alon Itai, and Matthew J Katz. Geometry helps in bottleneck matching and related problems. *Algorithmica*, 31(1):1–28, 2001.
- [3] Kaiming He, Xiangyu Zhang, Shaoqing Ren, and Jian Sun. Deep residual learning for image recognition, 2015.
- [4] Diederik P. Kingma and Jimmy Ba. Adam: A method for stochastic optimization, 2014.
- [5] Yuanzhi Li, Colin Wei, and Tengyu Ma. Towards explaining the regularization effect of initial large learning rate in training neural networks, 2019.
- [6] Leslie N. Smith. Cyclical learning rates for training neural networks, 2015.